J. Fluid Mech. (1997), *vol.* 340, *pp.* 35–59. Printed in the United Kingdom

Surfactant-induced retardation of the thermocapillary migration of a droplet

By JINNAN CHEN[1] AND KATHLEEN J. STEBE[2]†

[1] Beijing Institute of Technology, School of Chemical Engineering and Materials Science, PR China 100081

[2] Chemical Engineering Department, The Johns Hopkins University, Baltimore, MD 21218, USA

(Received 5 September 1995 and in revised form 18 December 1996)

A neutrally buoyant droplet in a fluid possessing a temperature gradient migrates under the action of thermocapillarity. The drop pole in the high-temperature region has a reduced surface tension. The surface pulls away from this low-tension region, establishing a Marangoni stress which propels the droplet into the warmer fluid. Thermocapillary migration is retarded by the adsorption of surfactant: surfactant is swept to the trailing pole by surface convection, establishing a surfactant-induced Marangoni stress resisting the flow (Barton & Subramanian 1990).

The impact of surfactant adsorption on drop thermocapillary motion is studied for two nonlinear adsorption frameworks in the sorption-controlled limit. The Langmuir adsorption framework accounts for the maximum surface concentration Γ'_∞ that can be attained for monolayer adsorption; the Frumkin adsorption framework accounts for Γ'_∞ and for non-ideal surfactant interactions. The compositional dependence of the surface tension alters both the thermocapillary stress which drives the flow and the surfactant-induced Marangoni stress which retards it. The competition between these stresses determines the terminal velocity U', which is given by Young's velocity U'_0 in the absence of surfactant adsorption. In the regime where adsorption–desorption and surface convection are of the same order, U' initially decreases with surfactant concentration for the Langmuir model. A minimum is then attained, and U' subsequently increases slightly with bulk concentration, but remains significantly less than U'_0. For cohesive interactions in the Frumkin model, U' decreases monotonically with surfactant concentration, asymptoting to a value less than the Langmuir velocity. For repulsive interactions, U' is non-monotonic, initially decreasing with concentration, subsequently increasing for elevated concentrations. The implications of these results for using surfactants to control surface mobilities in thermocapillary migration are discussed.

1. Introduction

The thermocapillary migration of a neutrally buoyant droplet in a fluid with a temperature gradient arises from the variation in surface tension with temperature. The droplet pole in the higher-temperature region has a reduced surface tension relative to elsewhere on the drop interface. The interface exerts a Marangoni stress, pulling away from the high-temperature pole. Viscous tractions provided by the internal and external fluids balance the Marangoni stress, creating a flow field which sends the drop in the direction of the temperature gradient. This phenomenon was first reported by Young, Goldstein & Block (1959) who demonstrated the thermocapillary migration of

† To whom correspondence should be addressed.

a bubble in a gravitational field using an air bubble suspended in a liquid. The suspending fluid formed a capillary bridge spanning an anvil. The lower anvil surface could be maintained at a higher temperature than the upper surface. The bubble, being less dense than the suspending liquid, rose in the absence of the applied temperature gradient. However, when the lower surface of the anvil was heated, the bubble could be held in position, i.e. the thermocapillary force exerted along the bubble interface was able to oppose buoyancy. In an analysis which neglects convective heat transport, (i.e. in the limit of zero thermal Péclet number), a theoretical expression for the temperature gradient required to immobilize a bubble in a gravitational field was derived and found to be in qualitative agreement with the bubble behaviour. The same theoretical framework can be used to find the terminal velocity U_0' of a surfactant-free drop or bubble moving under the action of thermocapillarity.

In the past decade there has been renewed interest in thermocapillary-driven flows because of the prospect of using thermocapillary drop migration as a means for removing droplets and bubbles in microgravity materials processing. Several review articles (Bratukin 1976; Hardy 1979; Subramaanian 1981, 1983, 1992; Wozniak, Siekmann & Srulijies 1988) have been published, which recapitulate the prior research on this subject. Below, only surfactant-related research in thermocapillary migration is reviewed.

Experiments have been conducted on liquid drops migrating in a vertical temperature gradient under the combined action of gravity and thermocapillarity by Lacy *et al.* (1982), Barton & Subramanian and Nallani & Subramanian (1992). In the experiments of Lacy *et al.*, the drop velocity was found to scale correctly with both the drop radius and the applied temperature gradient as predicted by Young *et al.* However, the velocities observed were less than the predicted value.

In order to probe whether surfactant adsorption could explain the observed retardartion, Barton & Subramanian performed drop migration experiments with and without the surfactant Triton-X 100 for the system of ethyl-salicylate droplets in a diethylene glycol continuous phase. In this system, the droplet phase is more dense than the continuous phase, so that in the absence of an applied temperature gradient, the droplet sank. When a temperature gradient was applied favouring drop rise, the droplets rose in the absence of added surfactant. Once the surfactant Triton-X 100 was added, however, the surface-driven thermocapillary force was sufficiently diminished that the gravity dominated, and the droplets sank even in the presence of the temperature gradient.

This experiment was modelled theoretically as a droplet moving in creeping flow with an insoluble surfactant monolayer by Kim & Subramanian (1989*a*, *b*). Assuming dilute surface concentrations, a linear surface equation of state relates the surface tension to the concentration of adsorbed surfactant. In Kim & Subramanian (1989*a*), the stagnant-cap limit was investigated, where surfactant swept to the trailing pole of the droplet creates a 'cap' region in which the Marangoni stresses are strong enough to stagnate the drop interface. Analytical solutions were obtained for the drop terminal velocity and the surfactant distribution. In Kim & Subramanian (1989*b*), surface diffusion redistributes surfactant on the interface, tending to oppose stagnant-cap formation. Depending on the ratio of characteristic surface convective to surface diffusive fluxes (i.e. the surface Péclet number for surfactant transport), a full range of behaviour can be realized. For small surface Péclet numbers, surfactant distributions vary only slightly from a uniform distribution on the interface, and the surface velocity is slightly retarded along the entire drop interface. At high surface Péclet number, stagnant-cap behaviour is approached.

In the experiments of Nallani & Subramanian, a drop of lesser density than the surrounding fluid was made to rise more rapidly by thermocapillary stresses. However, the enhancement in the rise velocity was less than that expected by Young's analysis for a surfactant-free interface. They used the stagnant-cap model of Barton & Subramanian to interpret their data, finding reasonable agreement between theory and experiment.

This paper addresses the surfactant-induced retardation of pure thermocapillary drop motion (i.e. in the absence of a gravitational field) in the limit of elevated surfactant concentration in the external fluid. In this limit, the mass transfer is ad/desorption-controlled. The linear model for the surface equation of state becomes inadequate when concentrations become appreciable because of such effects as monolayer saturation (accounted for in the Langmuir framework) and non-ideal surfactant interactions (included in the Frumkin framework). The temperature field and flow fields are modelled neglecting convective transport.

2. Problem statement

A neutrally buoyant spherical droplet of radius a' and viscosity $\mu'^{(1)}$ moves steadily under the action of thermocapillarity in an unbounded Newtonian fluid of viscosity $\mu'^{(2)}$. The origin of a spherical coordinate system (r', θ, ϕ), is located at the centre of the droplet, the angle θ being measured from the front stagnation point (see figure 1). In a droplet-fixed reference frame, the continuous phase far from the droplet moves with velocity U' in the $-z'$-direction. The outer fluid contains a surfactant at bulk concentration C'_{eq} which is immiscible in the droplet phase and possesses a constant temperature gradient $\nabla T'_\infty$ far from the droplet. The thermal conductivities for each phase are denoted by $\delta'^{(i)}$. (Here and throughout this article dimensional quantities are denoted with primes, dimensionless quantities are unprimed. Droplet quantities are denoted with superscript (1), continuous-phase quantities with superscript (2).) The non-uniform surfactant surface concentration Γ' and temperature T' create a variation in the surface tension γ' which is balanced by viscous shearing at the interface:

$$(\tau^{(2)'}_{r\theta} - \tau^{(1)'}_{r\theta})\,|_{r'=a'} = -\frac{1}{a'}\frac{\partial \gamma'}{\partial \theta} = -\frac{1}{a'}\frac{\partial \gamma'}{\partial T'}\frac{\partial T'}{\partial \theta}\bigg|_{r'=a'} - \frac{1}{a'}\frac{\partial \gamma'}{\partial \Gamma'}\frac{\partial \Gamma'}{\partial \theta}, \tag{1}$$

where $\tau^{(i)'}_{r\theta}$ denotes the shear stress of the drop ($i = 1$) or exterior phase ($i = 2$). The first term on the right-hand side of (1) is the thermocapillary stress which drives the flow; the second is the surfactant-induced Marangoni stress which resists the thermocapillary motion. The form of the adsorptive–desorptive fluxes determines the functional form of $\gamma'(\Gamma', T')$ in (1). In order to understand this dependence, first consider surfactant adsorption along a droplet in an isothermal environment. The adsorption flux is assumed to be first order in concentration C'_{eq}, and first order in space remaining on the interface, where Γ'_∞ is the upper bound on the surfactant concentration for monolayer adsorption. The desorption flux is first order in the surface concentration Γ'. The difference between adsorption and desorption fluxes is the net bulk flux to the interface:

$$-j'_r = \beta' C'_{eq}(\Gamma'_\infty - \Gamma') - \alpha'\Gamma', \tag{2}$$

where β' and α' are the kinetic constants for adsorption and desorption, respectively. These kinetic constants have an Arrhenius activation energy dependence:

$$\beta' = \beta'_0 \exp(-E'_a/R'T'), \tag{3}$$

$$\alpha' = \alpha'_0 \exp(-E'_d/R'T'), \tag{4}$$

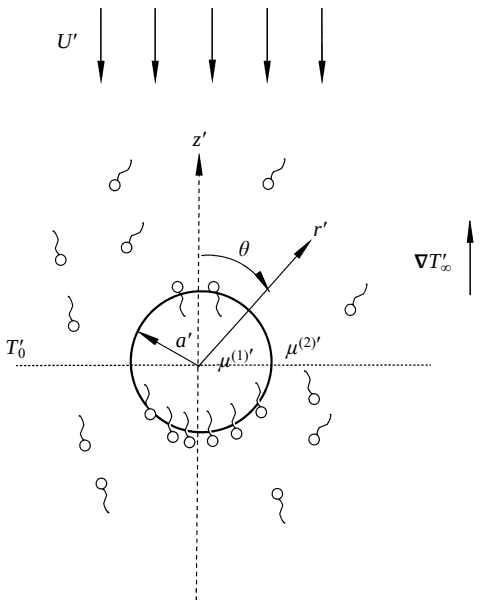

FIGURE 1. The droplet is depicted in a drop-fixed reference frame. The origin of a spherical coordinate system (r', θ, ϕ), is located at the centre of the droplet. The continuous phase moves with velocity U' in the $-z'$-direction under the action of thermocapillarity.

where $E'_a(E'_d)$ denotes the energy of activation for adsorption (desorption) and $R'T'$ is the product of the ideal gas constant and the temperature.

At equilibrium, the bulk flux in (2) is zero, and the equilibrium adsorption isotherm relating $\Gamma'_{eq}(C'_{eq})$ is obtained. If the activation energies are constant and denoted E'_{a0} and E'_{d0}, respectively, the Langmuir adsorption isotherm is obtained:

$$\frac{\Gamma'_{eq}}{\Gamma'_{\infty}} = \frac{k}{1+k}. \tag{5}$$

The adsorption number k, the ratio of the characteristic rates of adsorption to desorption, can be considered a dimensionless bulk concentration, where k is defined

$$k = \frac{\beta'_0 C'_{eq}}{\alpha'_0} \exp \frac{-(E'_{a0} - E'_{d0})}{R'T'}. \tag{6}$$

Non-ideal interactions among the adsorbed surfactant can create energy barriers to adsorption or desorption which depend upon surface concentration. If this dependence is linear, the energies can be expressed as

$$E'_i = E'_{i0} + \nu'_i \Gamma'_{eq}, \tag{7}$$

where the subscript $i = a, d$ denotes adsorption and desorption, respectively, and ν'_i is the slope of the activation energy with respect to surface concentration. At equilibrium, the Frumkin adsorption isotherm is obtained:

$$\frac{\Gamma'_{eq}}{\Gamma'_{\infty}} = \frac{k}{\exp\left(-\lambda \Gamma'_{eq}/\Gamma'_{\infty}\right) + k}, \tag{8}$$

where the interaction parameter λ is

$$\lambda = \frac{(\nu'_d - \nu'_a)\,\Gamma'_\infty}{R'T'}. \tag{9}$$

For inter-surfactant cohesion, the energy for desorption increases relative to that for adsorption, and $\lambda > 0$. The converse is true for repulsive interactions. Notice that when $\lambda = 0$ the Frumkin isotherm reduces to the Langmuir isotherm (i.e. no interactions).

The adsorption isotherms are graphed in figure 2(*a*). First consider the Langmuir framework. The surface concentration asymptotes to the maximum coverage Γ'_∞ at elevated k. The linear adsorption equation is shown to agree with $k \ll 1$ behaviour of the nonlinear frameworks, but it overpredicts the surface concencentration as k approaches 1. The curves for which λ is non-zero illustrate how non-ideal interactions alter the equilibrium distribution of surfactant. For a given bulk concentration of surfactant (i.e. k fixed), greater Γ'_{eq} values result for cohesive interactions among adsorbed surfactant, lesser Γ'_{eq} for repulsive interactions.

For the Frumkin framework, the surface equation of state relating γ'_{eq} to Γ'_{eq} is determined by the Gibbs adsorption equation to be

$$\gamma'_{eq} = \gamma'_0 + R'T'\Gamma'_\infty(\ln[1-\Gamma'_{eq}/\Gamma'_\infty] + \tfrac{1}{2}\lambda(\Gamma'_{eq}/\Gamma'_\infty)^2), \tag{10}$$

where γ'_0 is the surface tension of the surfactant-free interface. The surface equation of state for a Langmuir framework is obtained simply by equating λ to zero. The equations of state are shown in figure 2(*b*). A comparison of the Langmuir and linear frameworks show the effect of monolayer saturation. The linear asymptote to the equation of state overpredicts the reduction in the surface tension as k approaches unity.

The role of non-idealities is somewhat more complex. As λ increases from zero, the surface tension becomes less sensitive to the adsorbed surfactant concentration. However, the surface concentration realized for cohesion is much greater than that for no interactions or repulsion. This introduces an insensitive region in the surface tension graph at small k, where Γ'_{eq} is small, and the quadratic cohesion term nearly balances the logarithmic monolayer saturation term. At higher k, the surface tension decreases rapidly, as the higher Γ'_{eq} values realized cause the logarithmic term to dominate. Repulsive interactions increase the sensitivity of γ'_{eq} to Γ'_{eq}, but have lower Γ'_{eq} at a given k. The result is a shallow surface tension reduction curve, i.e. the surface tension is reduced less at a given k than for the no-interactions case. For a thorough discussion of the implications of non-ideal interactions in the dynamics of surfactant exchange, see Lin, McKeigue & Maldarelli (1994).

Because the droplet moves through a fluid with a temperature gradient, the local temperature environment changes as the drop translates. This is a quasi-steady study in which bubble location changes slowly so that the bubble reflects local averaged quantities evaluated at a reference temperature T'_0 for all of the system parameters except the surface tension. This reference temperature is equal to the temperature at the drop equator infinitely far from the drop.

In order to incorporate non-isothermal effects in the surface tension, (10) is expanded linearly in T' about T'_0:

$$\gamma'_{eq} = \gamma'_0|_{T'=T'_0} + R'T'\Gamma'_\infty(\ln[1-\Gamma'_{eq}/\Gamma'_\infty] + \tfrac{1}{2}\lambda(\Gamma'_{eq}/\Gamma'_\infty)^2) + \frac{\partial\gamma'_0}{\partial T'}(T'-T'_0). \tag{11}$$

The derivative $\partial\gamma'_0/\partial T'$ is the surface excess entropy of a pure material, which is always negative. The surface equation of state is assumed to be obeyed locally for a non-

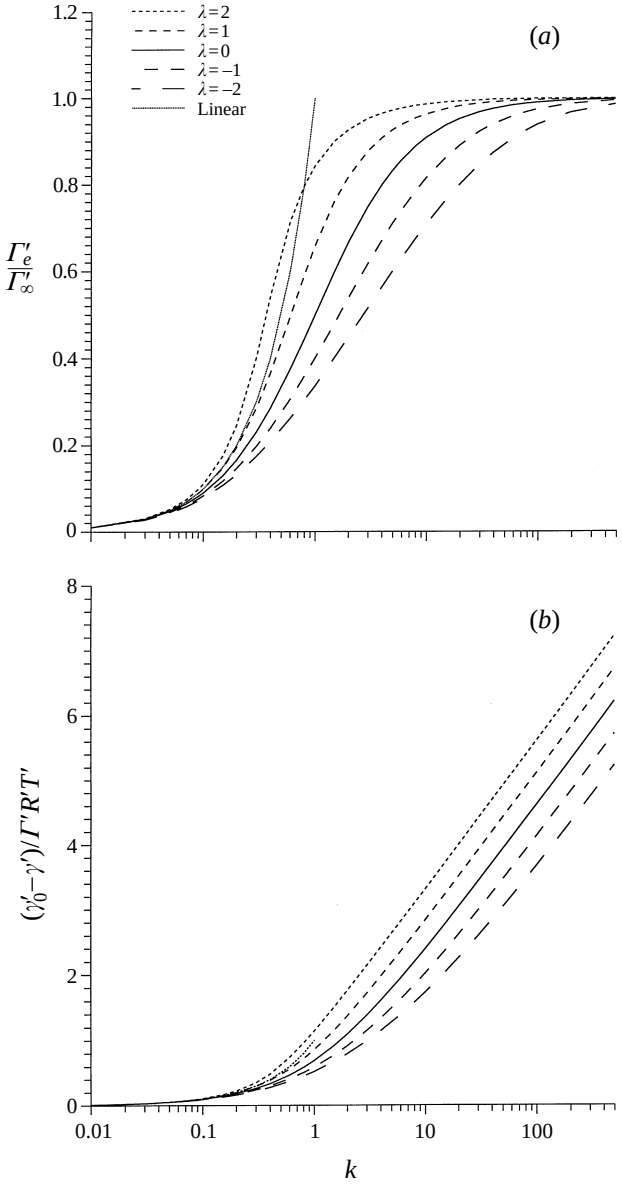

FIGURE 2. (*a*) The linear, Langmuir ($\lambda = 0$) and Frumkin $\lambda = 2, 1, -1, -2$ isotherms are graphed. For a given k value, the $\Gamma'_{eq}/\Gamma'_\infty$ values which result are greater for cohesion, and smaller for repulsion when compared to the Langmuir case. (*b*) The surface tension reduction $(\gamma'_0-\gamma'_{eq}/R'T'\Gamma'_\infty)$ for the linear, Langmuir Frumkin equations of state are plotted vs. k.

uniform Γ' so that γ' is related to Γ' and T' by (11). The derivative of this expression therefore determines the Marangoni stresses which develop:

$$\left.\begin{aligned} \frac{\partial\gamma'}{\partial T'} &= \frac{\partial\gamma'_0}{\partial T'} + R'\Gamma'_\infty(\ln[1-\Gamma'_{eq}/\Gamma'_\infty] + \tfrac{1}{2}\lambda(\Gamma'_{eq}/\Gamma'_\infty)^2), \\ \frac{\partial\gamma'}{\partial\Gamma'} &= R'T'\left(\frac{-1}{1-\Gamma'/\Gamma'_\infty} + \lambda\frac{\Gamma'}{\Gamma'_\infty}\right), \end{aligned}\right\} \tag{12}$$

where the parameters k, λ and Γ'_∞ are assumed independent of temperature. In (12), as Γ' approaches Γ'_∞ (i.e. as the interface approaches monolayer saturation), the temperature derivative becomes strongly negative, indicating that the γ' becomes increasingly sensitive to temperature at elevated surface concentrations. The surface concentration derivative also diverges, indicating that strong surfactant-induced Marangoni stresses develop which slow the surface convective flux of surfactant to the drop trailing pole, thereby stopping the surface concentration from reaching Γ'_∞.

Non-ideal interactions also impact the stresses which develop. For cohesion, surfactant finds it energetically favourable to accumulate: the interaction parameter $\lambda > 0$, and smaller Marangoni stresses (thermal or surfactant-induced) develop relative to the Langmuir or repulsive cases for identical Γ' distributions. However, on the moving droplet, λ strongly impacts the distributions realized because of the dependence of the sorption kinetics on the interactions: for $\lambda > 0$, α' decreases with Γ', producing greater Γ' gradients and stronger Marangoni stresses.

Through the interaction parameter λ, only the difference between ν'_d and ν'_a appears in the surface equation of state and isotherm. However, their individual values determine the adsorption and desorption kinetic constants, (3) and (4). In this study, we assume that ν'_a is zero, i.e. cohesion and repulsion are assumed to change the kinetics for desorption alone.

3. Governing equations in non-dimensional form

In order to cast the governing equations in dimensionless form, the velocity is scaled with U'_0, the migration velocity of a surfactant-free droplet in an infinite medium (Young *et al.*):

$$U'_0 = \frac{a'(-\partial\gamma'/\partial T')\,\nabla T'_\infty}{\mu^{(2)\prime}(1+3\kappa/2)(2+\delta)}, \tag{13}$$

where the ratio κ is the viscosity ratio of the droplet to the continuous phase:

$$\kappa = \mu^{(1)\prime}/\mu^{(2)\prime}, \tag{14}$$

and the ratio δ is the conductivity ratio of the droplet to the continuous phase:

$$\delta = \delta^{(1)\prime}/\delta^{(2)\prime}. \tag{15}$$

Lengths are scaled with the droplet radius a'; Γ' is made dimensionless with Γ'_{eq}; the bulk concentration of surfactant C' is scaled with C'_{eq}, the normal flux to the interface j'_r is scaled with $\Gamma'_{eq}U'_0/a'$, and the viscous stresses and pressure p' are made dimensionless with $\mu'^{(2)}U'_0/a'$. Surface tension gradients are scaled with $R'T'_0\Gamma'_\infty$.

Surfactant transport is considered in the limit where sorption kinetics between the sublayer and the interface are controlling. The temperature field is considered in the limit of negligible convective transport. The flow is considered in the creeping flow limit, and the droplet is assumed to remain spherical. The restrictions that these assumptions place on the system parameters in addition to the obvious restriction to negligible Reynolds number *Re* are detailed below.

The assumption that the droplet deformation is negligible is certainly valid if the system capillary number, the ratio of viscous stresses (which tend to deform the droplet) to surface tension (which resists deformation), is very small. However, under creeping flow conditions, drop deformation may not be important, even at finite

capillary number. Haj-Hariri *et al.* (1995) recently studied the droplet deformation in thermocapillary migration of droplets as a function of thermal Péclet number (termed the Marangoni number in their work). It was reported that increasing the Marangoni number alone does not lead to substantial deformations at $Re = 0$, even for capillary numbers on the order of unity. Nor has substantial deformation been reported in thermocapillary migration experiments. As reported by Subramanian (1992) in a recent review article, in no experiments reported for thermocapillary migration up to 1992, whether under the influence of gravity or in a low-gravity environment, has a measurable deformation in shape from a sphere been observed.

In both the drop and external-fluid phases a dimensional energy balance can be written:

$$\rho^{(i)\prime} C_p^{(i)\prime} \boldsymbol{v}^{(i)\prime} \cdot \boldsymbol{\nabla}' T^{(i)\prime} = \delta^{(i)\prime} \nabla^{2\prime} T^{(i)\prime} \tag{16}$$

where $C_p^{(i)\prime}$ is the specific heat capacity, $v^{(i)\prime}$ is the velocity field, $\rho^{(i)\prime}$ is the density and $\delta^{(i)}$ is the conductivity of the phase under consideration. A dimensionless temperature field is defined:

$$\Theta = \frac{T' - T'_0}{a' \boldsymbol{\nabla}' T'_\infty}. \tag{17}$$

Recast in dimensionless form, the energy balance is

$$\frac{1}{Pe_t^{(i)}} \boldsymbol{v}^{(i)} \cdot \boldsymbol{\nabla} \Theta^{(i)} = \nabla^2 \Theta^{(i)}, \tag{18}$$

where the thermal Péclet number for each phase $Pe_t^{(i)}$,

$$Pe_t^{(i)} = \frac{U'_0 a'}{\alpha'}, \quad \alpha' = \frac{\rho^{(i)\prime} C_p^{(i)\prime}}{\delta^{(i)\prime}}, \tag{19}$$

is the characteristic rate of convective heat transport to conductive transport. In our analysis, thermal Péclet numbers are assumed negligibly small, and the temperature field is governed by Laplace's equation:

$$\nabla^2 \Theta^{(i)} = 0. \tag{20}$$

In the absence of motion, surfactant adsorbs along the interface, establishing the surface concentration Γ'_{eq} and surface tension γ'_{eq}. Drop motion redistributes the surfactant: a steady non-equilibrium surface concentration Γ' develops when the surface convective flux toward the trailing pole of the droplet is balanced by the flux from the bulk (Levich 1962):

$$\boldsymbol{\nabla}'_s \cdot (\Gamma' \boldsymbol{v}'_s) - D'_s \nabla^2 \Gamma' = -j'_r. \tag{21}$$

In this expression, $\boldsymbol{v}'_s$ is the surface velocity, $\boldsymbol{\nabla}'_s$ is the surface gradient operator, D'_s is the surface diffusion coefficient and $-j'_r$ is the flux from the bulk toward the drop surface. In dimensionless form, the surface mass balance is

$$\boldsymbol{\nabla}_s \cdot (\Gamma \boldsymbol{v}_s) - \frac{1}{Pe_s} \nabla_s^2 \Gamma = -j_r, \tag{22}$$

where the surface Péclet number,

$$Pe_s = U'_0 a' / D'_s, \tag{23}$$

is the characteristic ratio of surface convective to surface diffusive transport. Surface diffusivities are typically of order $10^{-6}\,\mathrm{cm^2\,s^{-1}}$. For droplets of radius of 0.01 cm, typical U_0' are about $10^{-2}\,\mathrm{cm\,s^{-1}}$. For these values, Pe_s is typically order 100. In our analysis, it is assumed that Pe_s tends to infinity, and surface diffusion is neglected.

In general, the flux j_r' controlled by both diffusion flux of surfactant toward the interface, which establishes the sublayer concentration, and the subsequent partitioning of surfactant between the sublayer and the interface by adsorptive–desorptive exchange. The diffusion flux j_{rD}' is

$$j_{rD}' = D' \left.\frac{\partial C'}{\partial r'}\right|_{r'=a'}, \tag{24}$$

where the bulk concentration C' is uniform at C_{eq}' far from the droplet. In non-dimensional form, the diffusive flux becomes

$$j_{rD} = \frac{1}{Pe}\frac{1}{h}\left.\frac{\partial C}{\partial r}\right|_{r=1}, \tag{25}$$

where Pe is the bulk Péclet number, the ratio of characteristic bulk convective fluxes to bulk diffusive fluxes:

$$Pe = U_0' a'/D', \tag{26}$$

and h is the adsorption depth, a characteristic depth beneath the interface depleted by surfactant adsorption:

$$h = \Gamma_{eq}'/C_{eq}' a'. \tag{27}$$

As C_{eq}' increases, Γ' approaches its saturation value Γ_∞', and the adsorption depth h approaches zero. In order for the dimensionless diffusion flux to remain bounded in this limit, C becomes uniform, and the diffusion flux of surfactant becomes rapid even at large bulk Péclet number. In this limit, surfactant transport is governed by the adsorption/desorption flux between the sublayer and the interface.

Adopting these assumptions, bulk diffusion is instantaneous, maintaining a uniform bulk concentration, $C = 1$. The steady dimensionless surface mass balance expressed in spherical coordinates is

$$\frac{1}{\sin\theta}\frac{\partial}{\partial\theta}(\sin\theta\,\Gamma v_s) = Bi\left[k\left(\frac{1}{y}-\Gamma\right)-\Gamma\exp(-\lambda\Gamma y)\right], \tag{28}$$

where v_s is given by $v_\theta(\theta, r=1)$. In this expression, $y = \Gamma_{eq}'/\Gamma_\infty'$, given by (5) for the Langmuir model and by (8) for the Frumkin model. The Biot number is the ratio of characteristic desorptive fluxes to characteristic surface convective flux:

$$Bi = \frac{\alpha_0 \exp(-E_{a_0'}/R'T_0')\,a'}{U'}. \tag{29}$$

In dimensionless form, the tangential stress balance becomes

$$(\tau_{r\theta}^{(2)} - \kappa\tau_{r\theta}^{(1)})|_{r=1} = (1+3\kappa/2)(2+\delta)\left[E(G\theta+1)\left(\frac{y}{1-\Gamma y}-\lambda\Gamma y^2\right)\frac{\partial\Gamma}{\partial\theta}\right.$$
$$\left.-[EG(\ln(1-\Gamma y)+\tfrac{1}{2}\lambda\Gamma^2 y^2)-1]\frac{\partial\Theta}{\partial\theta}\right], \tag{30}$$

where the elasticity number E is a ratio of characteristic surfactant-induced Marangoni stresses which resist the droplet motion to the characteristic (surfactant-free) temperature-induced Marangoni stresses which drive the flow:

$$E = \frac{R' T_0' \Gamma_\infty'}{a'(-\partial\gamma_0'/\partial T')\,\nabla T_\infty'}. \tag{31}$$

Finally, G is a characteristic normalized temperature gradient across the droplet:

$$G = \nabla T_\infty' a'/T_0'. \tag{32}$$

Attention is restricted to $G \ll 1$ because of the assumption of linear dependence of the surface tension on the temperature field, and the fact that temperature dependence of the other system parameters has been neglected.

The boundary conditions on the temperature fields are:

(i) the heat flux and temperature are continuous across the drop interface

$$\delta \frac{\partial \Theta^{(1)}}{\partial r} = \frac{\partial \Theta^{(2)}}{\partial r}, \quad \Theta^{(1)} = \Theta^{(2)}; \tag{33}$$

(ii) far from the drop, the temperature field in the continuous phase is linear in z

$$\lim_{|r|\to\infty} \Theta^{(2)} = z; \tag{34}$$

(iii) at the centre of the sphere the temperature is finite.

The solution for the temperature field is straightforward (see Young *et al.*), yielding the external and internal temperature fields:

$$\Theta^{(1)} = r\cos\theta \frac{3}{2+\delta}, \quad \Theta^{(2)} = r\cos\theta + r^{-2}\cos\theta \frac{1-\delta}{2+\delta}. \tag{35}$$

For an axisymmetric and incompressible flow, velocities may be represented by a stream function Ψ', which is scaled with $a'^2 U_0'$. Stokes' equations for steady axisymmetric creeping flow in terms of the stream function are

$$\mathrm{E}^2(\mathrm{E}^2\psi^{(i)}) = 0, \tag{36}$$

where E^2 is the axisymmetric stream function operator in spherical coordinates:

$$\mathrm{E}^2 = \frac{\partial^2}{\partial r^2} + \frac{\sin\theta}{r^2}\frac{\partial}{\partial\theta}\left(\frac{1}{\sin\theta}\frac{\partial}{\partial\theta}\right). \tag{37}$$

The velocity components in terms of the stream function are

$$v_r^{(i)} = -\frac{1}{r^2\sin\theta}\frac{\partial\psi^{(i)}}{\partial\theta}, \quad v_\theta^{(i)} = \frac{1}{r\sin\theta}\frac{\partial\psi^{(i)}}{\partial r}. \tag{38}$$

The general form of the solution of (36) in spherical coordinates can be found by separation of variables to be

$$\Psi^{(i)}(r,\theta) = \sum_{n=0}^{\infty} (A_n^{(i)} r^n + B_n^{(i)} r^{-n+1} + C_n^{(i)} r^{n+2} + D_n^{(i)} r^{-n+3})\, Q_n^{-1/2}(\cos\theta), \tag{39}$$

where $i = 1, 2$ respectively and $Q_n^{-1/2}(\cos\theta)$ is the Gegenbauer polynomial of degree $-1/2$ and order n. The unknown coefficients in this series expansion are determined by the boundary conditions, enumerated below.

(i) Far from the droplet, the uniform velocity field requires that the stream function obey

$$\lim_{r\to\infty} \psi^{(2)} = \tfrac{1}{2} U r^2 \sin^2\theta. \tag{40}$$

(ii) At the droplet centre $v_r^{(1)}$ and $v_\theta^{(1)}$ exist.

(iii) At droplet surface, the tangential velocity components must be continuous:

$$v_\theta^{(1)}(1,\theta) = v_\theta^{(2)}(1,\theta). \tag{41}$$

(iv) The normal velocities are zero at the interface:

$$v_r^{(1)}(1,\theta) = v_r^{(2)}(1,\theta) = 0. \tag{42}$$

(v) Since the droplet is assumed *a priori* to remain spherical, the normal stress balance on the interface is replaced by an integral force balance to find F_z', the net drag exerted on the particle. For the stream function form in (39) F_z' reduces to (Happel & Brenner 1973)

$$F_z' = 4\pi\mu^{(2)\prime} U' D_2^{(2)}. \tag{43}$$

For thermocapillary migration in the absence of body forces, the viscous stress and surfactant-induced stresses resisting the droplet motion are balanced by thermocapillary stress which drives the flow. Thus, at steady state, the net force on the droplet is zero, and $D_2^{(2)} = 0$.

(vi) The tangential stress jump at the interface is balanced by the Marangoni stress, as expressed in (30).

The surface concentration Γ is coupled to the flow field by the surface mass balance (28) and the tangential stress balance (30). The flow field is coupled with the temperature field (35) through the tangential stress (30). The fluid mechanics equations and the surface mass balance must be solved simultaneously to find the flow field and surfactant distribution. The solution technique is detailed in the Appendix to this article.

4. Results and discussion

Several of the parameters governing the system behaviour have been varied to confirm that expected limits are recovered. For example, the system was studied as a function of the conductivity ratio δ and the viscosity ratio κ. As δ becomes large, the temperature gradient over the droplet interface disappears, and the droplet interfacial motion is arrested. The effects of κ on the flow field are discussed in greater detail in §4.6. Surfactant effects are discussed in §§4.1–4.5 for $\kappa = 0$.

The surfactant-related parameters include the elasticity number E, the Biot number Bi, the adsorption number k and the non-ideality parameter λ. The results are discussed first for the case in which surfactant molecules do not interact, $\lambda = 0$, and the surfactant is described by the Langmuir adsorption framework.

4.1. *Langmuir results*

The Γ and Marangoni stress profiles are shown in figures 3(*a*) and 3(*b*), respectively. The corresponding v_s profile and terminal velocity ratio U are shown in figures 4(*a*) and 4(*b*), respectively. First consider the $Bi = 1.0$ results which are shown for the Langmuir and linear frameworks. The linear isotherm strongly overpredicts the Γ' gradients

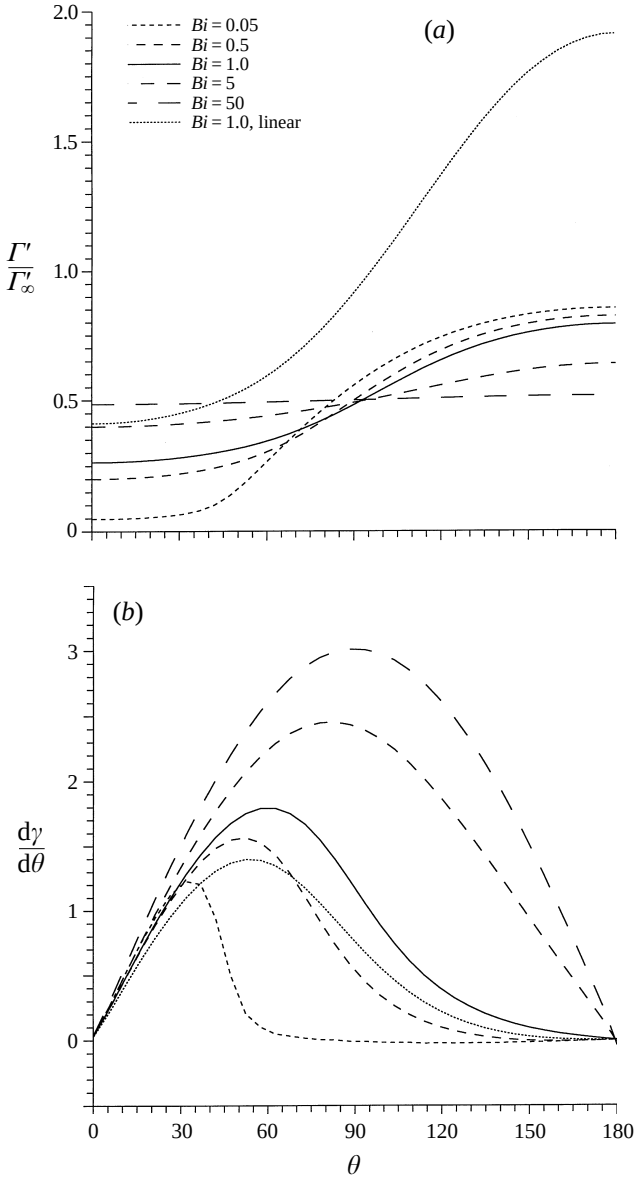

FIGURE 3. (*a*) The $\Gamma'(\theta)/\Gamma'_\infty$ profies and (*b*) the Marangoni stress profiles for the Langmuir framework as a function of Bi for $k = 1.0$, $E = 1.0$, $G = 0.05$ and $\delta = 1$. Curves are plotted for $Bi = 0.05$, 0.5, 1, 5, 50, and for the linear isotherm at $Bi = 1.0$.

realized, because there is no upper bound on Γ' in this model. In contrast, none of the nonlinear results allow Γ' to reach Γ'_∞. In this flow, a positive Marangoni stress indicates that the interface pulls from the front to the back pole, propelling the drop upward. The linear isotherm overpredicts the surfactant-induced reduction in this driving stress.

At elevated Bi, the terminal velocity approaches Young's velocity, and U approaches 1. In this limit, adsorption–desorption is rapid relative to the surface convective flux, and the surface concentration is maintained close to its uniform, equilibrium value. As Bi is decreased, however, the gradients in surface concentration become pronounced,

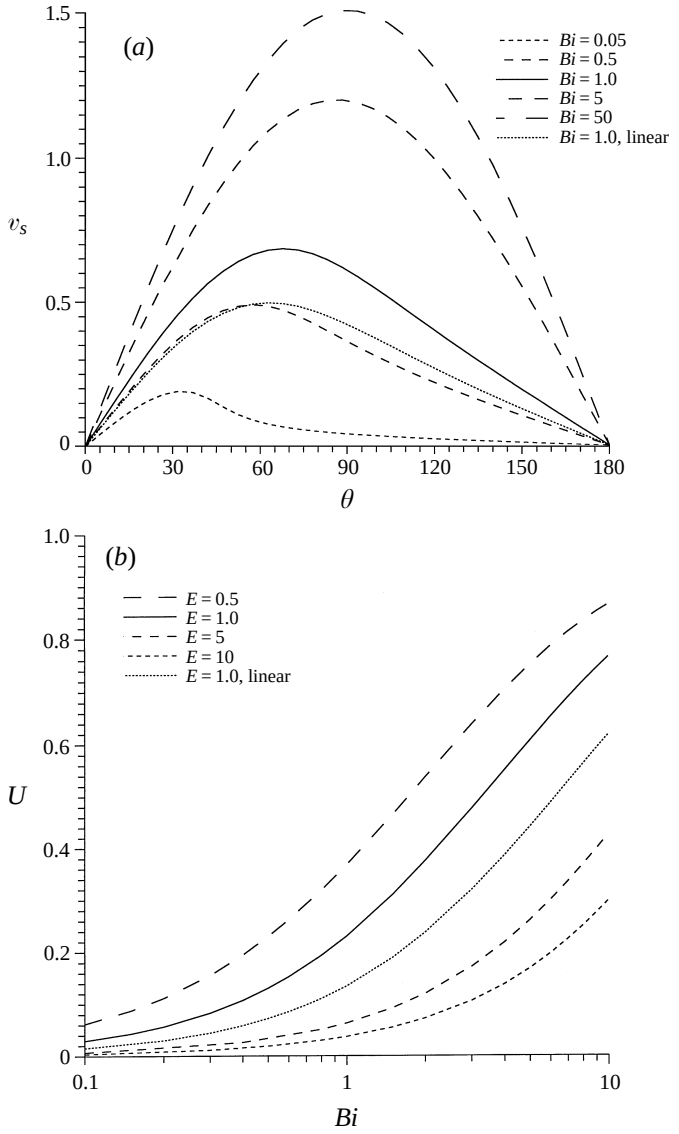

FIGURE 4. (*a*) The surface velocity profile $v_s(\theta)$ as a function of Bi at $k = 1.0$, $E = 1.0$, $G = 0.05$ and $\delta = 1$, for the Langmuir framework. Curves are plotted for $Bi = 0.05$, 0.5, 1, 5, 50 and for the linear isotherm at $Bi = 1.0$. (*b*) The terminal velocity ratio U vs. Bi as a function of E for $k = 1.0$, $G = 0.05$ and $\delta = 5$. Curves are plotted for $E = 0.5$, 1.0, 5.0, 10, and for the linear isotherm at $E = 1.0$.

producing strong surfactant-induced Marangoni stresses retarding the surface flow. At $Bi = 0.05$, stagnant-cap behaviour is approached, with the surface concentration being significantly depleted at the leading end of the drop and significantly enriched at the trailing end. The thermocapillary effect is able to create a surface tension gradient to drive a surface flow only at the leading portion of the droplet. At all other regions of the interface, v_s departs only slightly from zero. In this limit, U is strongly retarded. Figure 4(*b*) also shows the impact of the elasticity number E. As E is increased, the coupling between the surfactant distribution and the droplet motion becomes more pronounced.

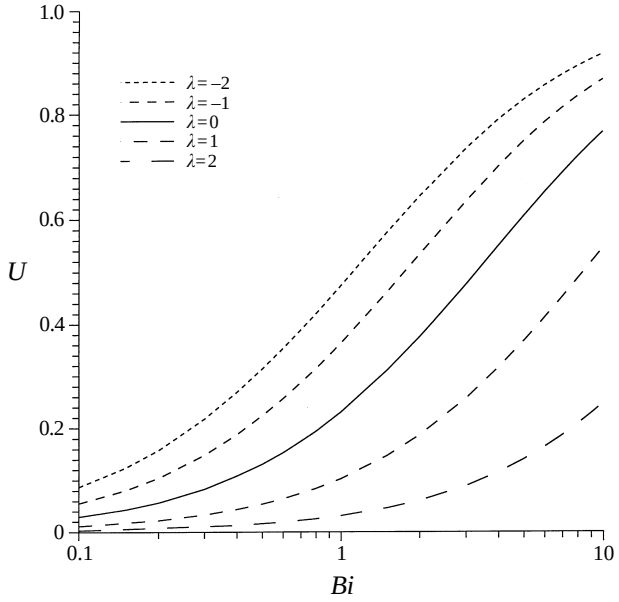

FIGURE 5. The terminal velocity ratio U vs. Bi as a function of λ for the Frumkin framework at $k = 1$, $E = 1.0$, $G = 0.05$ and $\delta = 5$. Curves are plotted for $\lambda = -2, -1, 0, 1, 2$.

The group G defined in (32), appears in the dimensionless tangential stress balance (30) as a factor both for the temperature in the surfactant-induced stress and for the surfactant-dependent part of the thermocapillary stress. In this study, only the G values of 0.05 and 0.1 were considered. The greater is G, a dimensionless characteristic thermal gradient across the droplet, the greater is the migration velocity. For example, for $k = 1.0$, $\kappa = 0$, $Bi = 1.0$, $E = 1.0$ and $\lambda = 0$, the terminal velocity increased slightly with G: $U(G = 0.05) = 0.4104$, while $U(G = 0.1) = 0.4252$.

4.2. *Frumkin framework results*

Non-ideal interactions alter surfactant behaviour in three ways. For cohesion, greater $\Gamma'_{eq}/\Gamma'_{\infty}$ values result at fixed k; the sensitivity of the surface tension to Γ' decreases; and the desorption coefficient α' decreases. The opposite trends hold for repulsion. In order to understand the impact of these interactions, the terminal velocity for the droplet was studied at fixed k for various λ values. The results are shown in figure 5; cohesion ($\lambda > 0$) reduces U, and repulsion ($\lambda < 0$) increases U at fixed bulk concentration. However, the amount of surfactant on the interface for the different λ values differs strongly; the decrease in U might be attributable to this alone. In order to separate this effect from the surface tension dependence and desorption dynamic effects, the droplet was studied at fixed mass of adsorbed surfactant:

$$\int_0^{\pi} \Gamma'(\theta)/\Gamma'_{\infty} \sin\theta \, \mathrm{d}\theta = 0.8, \tag{44}$$

corresponding to an average surface coverage of 0.4. The results for fixed adsorbed mass for $\Gamma'(\theta)/\Gamma'_{\infty}$ and the Marangoni stress are presented in figures 6(a) and 6(b), respectively. The corresponding $v_s(\theta)$ profiles are given in figure 7(a). Finally, U vs. λ is graphed in figure 7(b). These figures show that increasing λ favours stronger surface concentration gradients which reduce the thermocapillary stress that drives the flow.

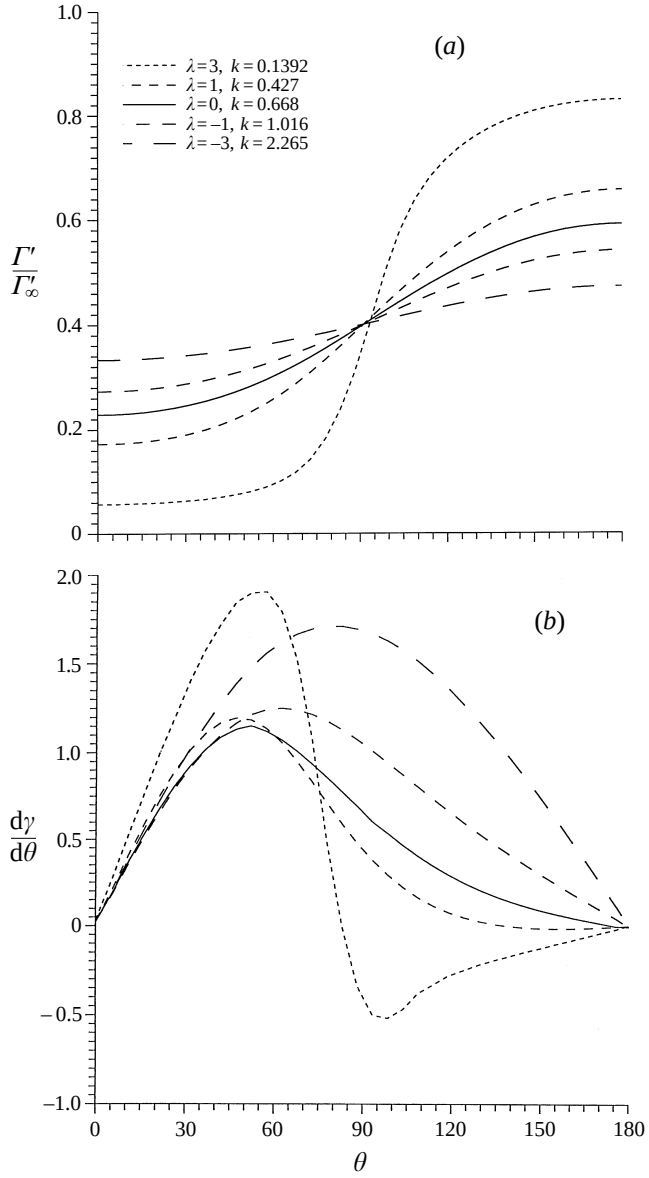

FIGURE 6. (*a*) The profiles for Γ'/Γ'_∞ and (*b*) the Marangoni stress for $\lambda = 3, 1, 0, -1, -3$ for fixed surface mass, $Bi = 1$, $E = 1$, $G = 0.05$ and $\delta = 5$.

The surface velocity and the terminal velocity are therefore retarded. The effect of λ on the flow is pronounced: for strong cohesion ($\lambda = 3$), the surface tension gradient actually reverses direction at the trailing end of the droplet, where the surfactant-induced stress dominates. The surface velocity is strongly retarded, and is reduced to $U = 0.15$. In contrast, for repulsion ($\lambda = -3$), weak surface concentration gradients are realized, and $U = 0.57$.

The strong retardation exhibited for cohesive interactions results from the desorption rate α', which shows as Γ' increases. Thus, the desorption rate at the rear pole slows as surfactant accumulates there, favouring further accumulation. Conversely, for repulsion, areas of higher surface concentration have faster desorption kinetics,

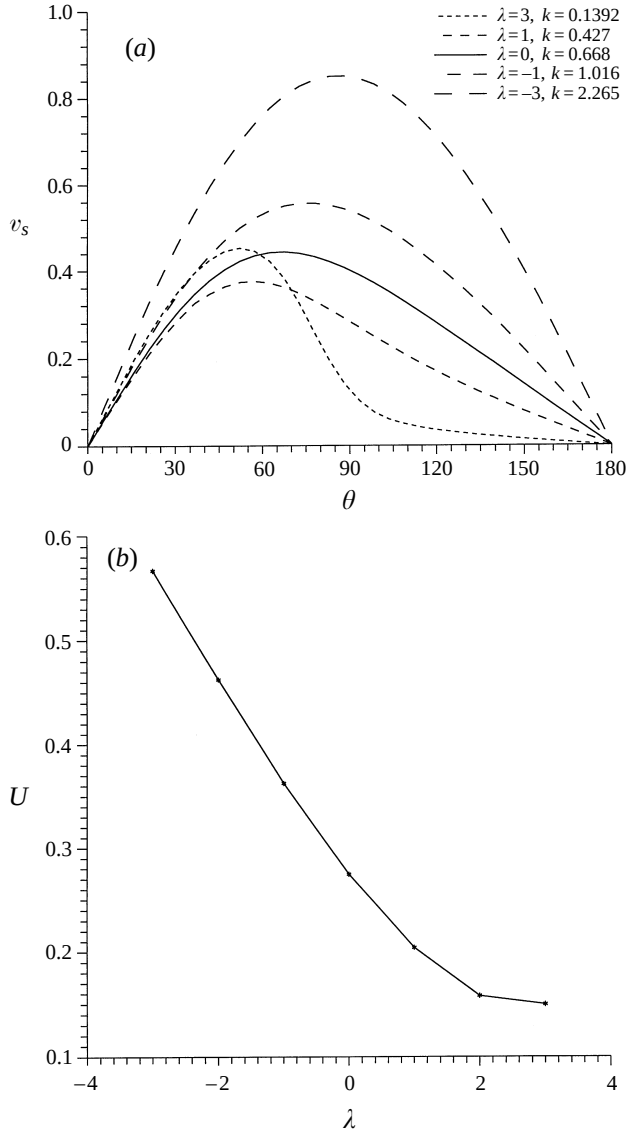

FIGURE 7. (*a*) The surface velocity profile $v_s(\theta)$ for $\lambda = 3, 1, 0, -1, -3$ for fixed surface mass, $Bi = 1$, $E = 1$, $G = 0.05$ and $\delta = 5$. (*b*) The terminal velocity ratio U vs. λ for fixed surface mass, $Bi = 1$, $E = 1$, $G = 0.05$ and $\delta = 5$.

favouring a uniform surfactant distribution on the surface. As a result, cohesive interactions act to strongly retard a surface flow, and repulsive interactions act to resist this retardation.

4.3. *Surface remobilization*: *using surfactants to control thermocapillary motion*

Surface remobilization is unretarded free-surface flow at elevated bulk surfactant concentration. Remobilization can be realized with a surfactant whose adsorption–desorption rates are rapid compared to the surface convective flux (i.e. *Bi* infinite). For these surfactants, the adsorption depth h defined in (27) can be forced to zero as the bulk concentration is made large, and the surface concentration can be made uniform.

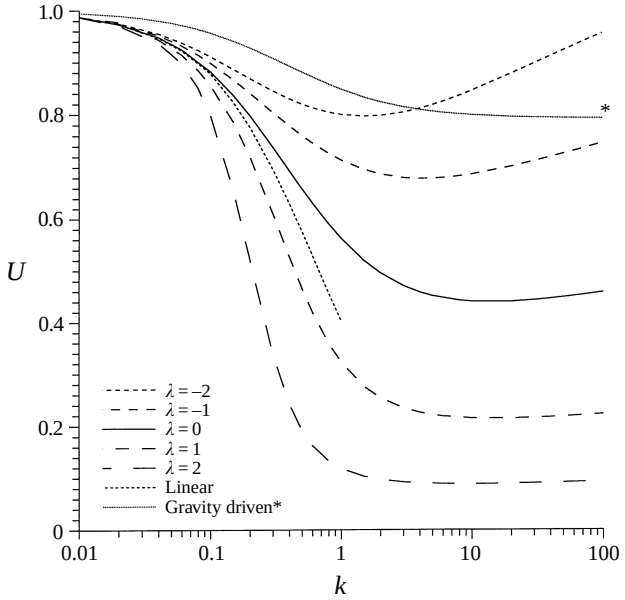

FIGURE 8. The terminal velocity ratio U vs. k as a function of λ for the Frumkin framework at $Bi = 3$, $E = 1.0$, $G = 0.05$ and $\delta = 3$. Curves are plotted for $\lambda = -2, -1, 0, 1, 2$ and the linear framework. In addition, the terminal velocity ratio for a gravity-driven droplet for the same surfactant physical chemistry ($Bi = 3$, $E = 1.0$) is shown.

Thus, the surface remains free of surfactant-induced Marangoni stresses, and the drop interface should be restored to a mobile condition. The arguments behind restored surface motion are detailed in Stebe, Lin & Maldarelli (1991), Stebe & Maldarelli (1994), and briefly reviewed in Chen & Stebe (1996).

The conditions for remobilization are met at large Bi and large k. However, the large-k behaviour of U at finite Bi indicates the degree of restored free interfacial motion that can be obtained at finite adsorption–desorption kinetics. The results in figure 8 for $Bi = 3.0$ show that the cohesive interactions ($\lambda = 2$) asymptote to $U = 0.05$, indicating that, as Γ' approaches Γ'_∞, α' is sufficiently slow that appreciable surfactant-induced Marangoni stresses develop to strongly resist the flow.

For the Langmuir case, a minimum in the U vs. k profile is reached; U subsequently increases weakly with k. This non-monotonic behaviour can be attributed to the $\ln(1-\Gamma'/\Gamma'_\infty)$ term in the thermocapillary stress driving the flow, which becomes stronger as the maximum surface packing limit is approached.

Finally, the droplet is nearly restored to free-surface flow at $k = 100$ for strong repulsion, $\lambda = -2$. This is attributable primarily to the desorption constant α', which becomes rapid as the surface concentration increases toward Γ'_∞. These results indicate that surface remobilization at elevated bulk concentration is favoured by repulsion and resisted by cohesion.

4.4. *Comparison to retardation of a settling droplet*

Recently, a related study of the impact of surfactant adsorption on the terminal velocity of droplets settling in a gravitational field has been performed (Chen & Stebe 1996). For gravity-driven flow, the complete stagnation of the droplet interface does not prevent drop motion, but rather the droplet settles at Stokes' velocity. The complete stagnation of an interface in pure thermocapillary-driven motion, however,

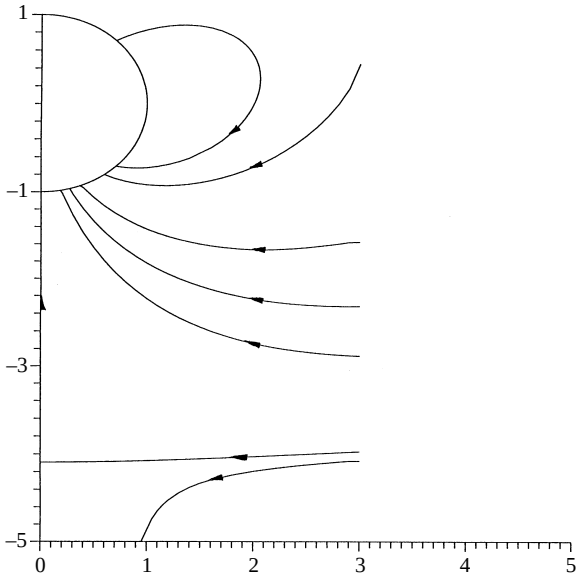

FIGURE 9. The streamlines for the Langmuir framework at $Bi = 3$, $E = 1.0$, $G = 0.05$, $\delta = 3$, and $k = 1$.

completely arrests the flow. Therefore, the reduction in the terminal velocity caused by surfactant adsorption in thermocapillary-driven drop motion is greater than that realized in the gravity-driven flow for the same surface equation of state. A comparison between the results from the two studies is shown in figure 8, where the reduction in the terminal velocity (scaled by Stokes' velocity) of a droplet settling under gravity at identical Bi and E for a surfactant described by the Langmuir formalism is presented. At $k = 100$, the settling droplet moves with roughly 80% of its unretarded velocity, but the corresponding thermocapillary-driven flow moves with only roughly 46% of its unretarded velocity.

4.5. *Streamlines*

Shankar & Subramanian (1988) studied finite convective thermal transport in drop thermocapillary motion, which disrupts the fore–aft symmetry of this flow. They presented the streamlines in a laboratory-fixed reference frame, revealing recirculating regions which were generated behind the droplet.

In the current problem, surfactant accumulation at the trailing pole of the drop disrupts fore–aft symmetry. Typical streamlines for the Langmuir adsorption framework are shown in figure 9. As in the flow configuration of Shankar & Subramanian, a separatrix streamline cuts across the flow. The streamlines are toward the droplet above the separatrix streamline, and away from the droplet below the separatrix streamline. This may influence issues such as particle–particle interactions, in that particles far from the drop or bubble are convected toward the particle above the separatrix, and convected away from it below. In table 1, the location of the separatrix streamline on the drop axis (z_{sep}) is tabulated from the linear, Langmuir and Frumkin frameworks as a function of k under the conditions reported in figure 9.

First consider the separatrix location for the Langmuir framework. U decreases monotonically for k less than 50. However, z_{sep} is not monotonic in k: first it approaches the droplet for $k < 1$, and then it migrates away. Therefore, this distance is not determined solely by the droplet terminal velocity. Rather, at $k < 1$, increasing k

	$\lambda = 0$		$\lambda = 2$		$\lambda = -2$	
k	U	$-z_{sep}$	U	$-z_{sep}$	U	$-z_{sep}$
0.1	0.8823	7.785	0.7991	3.749	0.9110	12.5054
0.5	0.6585	4.014	0.1909	1.406	0.8200	12.4845
1.0	0.5623	4.091	0.1183	1.927	0.8001	17.1212
5.0	0.4511	5.972	0.0891	3.315	0.8180	47.4059
10	0.4400	6.755	0.0882	3.516	0.8448	71.2642
50	0.4481	7.408	0.0911	3.541	0.9216	—
100	0.4578	7.356	0.0932	3.480	0.9547	—

TABLE 1. The axial location of the separatrix streamline as a function of k for the Langmuir framework ($\lambda = 0$), cohesion ($\lambda = 2$), and repulsion ($\lambda = -2$) for $Bi = 3$, $E = 1.0$, $G = 0.05$ and $\delta = 3.0$

increases the gradients realized in the surface concentration and in the surface velocity, strongly disrupting the droplet fore–aft symmetry. At higher bulk concentrations, the surface is increasingly sensitive to surface concentration gradients. (This is evident from the tangential stress balance (30) when y is expressed in terms of k.) The surface velocity reduces strongly for smaller surface concentration gradients. The reduced surface convective flux therefore leads to smaller Γ gradients in the steady-state distribution. The Γ profiles are presented as a function of k in figure 10(a), the corresponding surface velocity profiles are shown in figure 10(b). Because of the strong coupling, U is significantly retarded by a smaller disruption of fore–aft symmetry. Finally, for $k > 20$, the small inward migration of the separatrix location can be attributed to the $\ln(1-\Gamma'/\Gamma'_\infty)$ term in the thermocapillary stress, which slightly increases v_s and the Γ gradients.

A similar explanation holds for the cohesive-interactions case, save that the effective Biot number Bi_{eff},

$$Bi_{eff} = Bi \exp(-\lambda\Gamma), \tag{45}$$

decreases from 3 to about 0.4 for the results reported here, favouring stronger disruptions from fore–aft symmetry at all k than the Langmuir result. Thus, the separatrix is always closer to the droplet than for the Langmuir case.

The distance from the droplet of the separatrix streamline for the repulsive case increases monotonically with k. For this case, Bi_{eff} increases with bulk concentration to a maximum value of about 20. The desorption flux becomes rapid relative to the surface convective flux, and the surface concentration departs only slightly from its equilibrium value along the interface. Under these conditions, the fore–aft symmetry of the droplet is greater than for the corresponding Langmuir and cohesive cases and the separatrix distance is always further from the droplet.

4.6. *The effect of droplet viscosity*

The above discussion is for the viscosity ratio κ of zero. However, the migration velocity results apply regardless of κ. The viscosity ratio was varied in the simulations; its effect on the dimensionless terminal velocity (normalized by Young's migration velocity (13)) were very slight. That is, the κ dependence in Young's migration velocity holds even when there are significant Marangoni effects. For example, in table 2, the dimensionless terminal velocity U and separatrix location z_{sep} are tabulated as a function dimensionless concentration k for viscosity ratios $\kappa = 0$ and 0.5 for $Bi = 3$, $E = 1.0$, $G = 0.05$ and $\delta = 3$. The separatrix location is slightly closer to the viscous droplet, but the migration velocity is nearly unchanged. The insensitivity of the

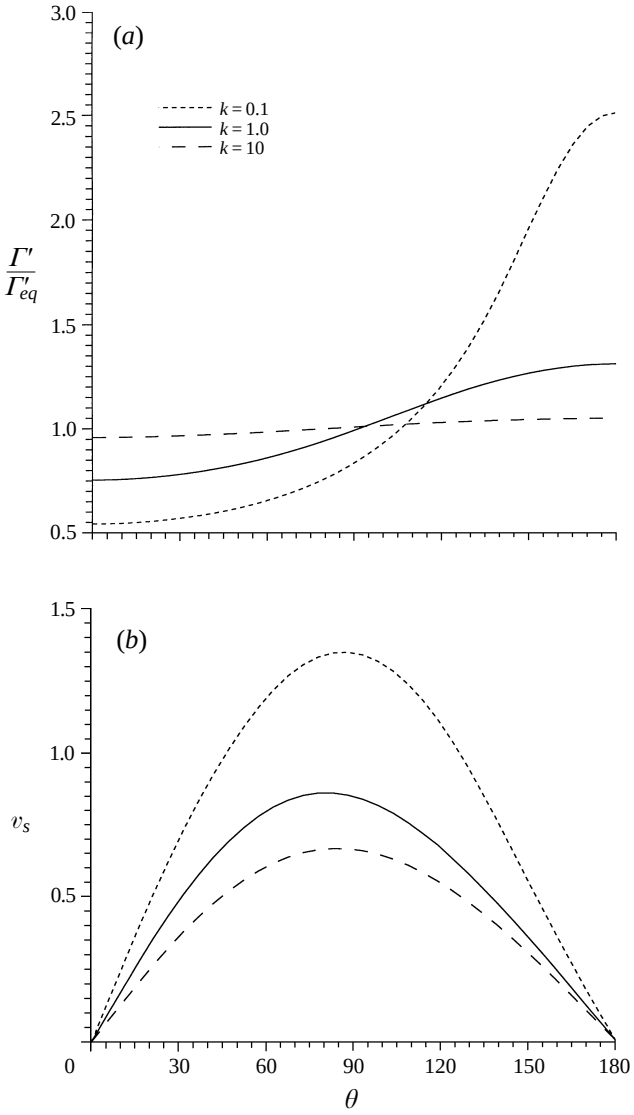

FIGURE 10. (*a*) The profiles for Γ'/Γ'_{eq} and (*b*) the surface velocity profile $v_s(\theta)$ for the Langmuir framework at $k = 0.1$, 1.0 and 10 for $Bi = 3$, $E = 1$, $G = 0.05$ *and* $\delta = 3$.

k	$U\ (\kappa = 0)$	$-z_{sep}\ (\kappa = 0)$	$U\ (\kappa = 0.5)$	$-z_{sep}\ (\kappa = 0.5)$
0.1	0.8823	7.785	0.8824	6.904
0.5	0.6585	4.014	0.6589	3.687
1.0	0.5623	4.091	0.5627	3.809
5.0	0.4511	5.972	0.4513	5.661
10	0.4402	6.755	0.4402	6.423
50	0.4481	7.408	0.4484	7.063
100	0.4578	7.356	0.4580	7.0165

TABLE 2. The axial location of the separatrix streamline as a function of k for the Langmuir framework ($\lambda = 0$), cohesion ($\lambda = 2$), and repulsion ($\lambda = -2$) for $Bi = 3$, $E = 1.0$, $G = 0.05$ and $\delta = 3.0$

κ	U
0	0.5623
0.5	0.5628
1.0	0.5628
2.0	0.5630
5.0	0.5631

TABLE 3. The terminal velocity ratio U as a function of λ for $k = 1.0$ for the Langmuir framework for $Bi = 3$, $E = 1.0$, $G = 0.05$ and $\delta = 3$, and various κ values

dimensionless migration velocity to the viscosity of the bulk fluid is further demonstrated in table 3, where U changes by less than 3 % when κ is varied from zero to 5 at fixed k at the same parameter values.

5. Conclusions

Surfactant effects on the thermocapillary motion of droplets were studied at elevated bulk surfactant concentrations for which the mass transfer is adsorption limited and the adsorption isotherm and equation of state are nonlinear.

The Langmuir model accounts for monolayer saturation, i.e. that there is an upper bound on the surface concentration that can be realized for monolayer coverage. The linear model has no such upper bound, and strongly overpredicts the surface concentration gradients and retardation of the flow in comparison to the Langmuir results.

The role of non-ideal interactions among adsorbed surfactant was probed using the Frumkin adsorption framework for the case where the adsorbed mass of surfactant is held constant. Cohesive interactions are shown to strongly retard the desorption rate as the surface concentration approaches maximum coverage, and significantly greater retardation of the thermocapillary flow results. Conversely, repulsive interactions among surfactants facilitate desorption from the interface. Thus, lower surface concentration gradients result, and the thermocapillary migration velocity is less reduced than for the corresponding Langmuir case.

Remobilization is a paradigm for controlling surface mobilities at elevated bulk concentrations in the infinite-Bi limit. At finite Bi, the terminal velocity realized at elevated k for Langmuir and Frumkin isotherms indicates the fastest terminal velocity that can be attained by adding a surfactant at elevated concentrations.

At finite Bi, the migration velocity for the Langmuir framework falls to a retarded value at elevated k. (A small upward trend in U with concentration is observed because of the enhanced sensitivity of the thermocapillary effect as the surface concentration approaches its upper bound.)

The Frumkin isotherm shows non-monotonic behaviour in U with k for repulsion. The terminal velocity decreases initially with k, subsequently increasing as Bi_{eff} increases as Γ' approaches Γ'_{∞}. For strong repulsive interactions, Bi_{eff} can increase significantly above Bi, and this non-monotonic behaviour is pronounced. Cohesive interactions yield monotonically decreasing U which asymptote to U less than unity at large k. Thus, the amount of free-surface motion that can be restored at elevated bulk concentrations is greater for repulsive interactions and less for cohesive interactions.

Recirculating regions in the flow in the laboratory-fixed frame indicate the degree of disruption of fore–aft symmetry, which is not related simply to the degree of surface

retardation. The role of non-ideal interactions is pronounced: repulsion favours fore–aft symmetry through rapid desorption kinetics and recirculating regions are far from the droplet; cohesion favours greater Γ gradients through slower desorption kinetics, and recirculating regions are closer to the droplet.

Finally, the effects of viscosity on the dimensionless migration velocity are extremely slight. For any given degree of surfactant-induced surface retardation, the dimensionless migration velocity is reduced. However, the magnitude of this reduction is insensitive to changes in the viscosity ratio. This implies that viscous effects are well described by the viscous drag at surfactant-free interfaces, included in Young's migration velocity U_0', which was used to normalize the dimensionless migration velocity.

Appendix. Solution technique

After the boundary condition (34) specifying boundedness at the drop centre and (40)–(42) are applied to (39), the stream function can be rewritten in terms of the unknown coefficients $B_n^{(2)}$:

$$\Psi^{(1)}(r,\theta) = \sum_{n=2}^{\infty} B_n^{(2)}(r^n - r^{n+2})\, Q_n^{-1/2}(\cos\theta) - \tfrac{1}{4}U(r^2 - r^4)\sin^2\theta, \tag{A 1}$$

$$\Psi^{(2)}(r,\theta) = \sum_{n=2}^{\infty} B_n^{(2)}(r^{-n+1} - r^{-n+3})\, Q_n^{-1/2}(\cos\theta) + \tfrac{1}{2}U(r^2 - r)\sin^2\theta. \tag{A 2}$$

The surface velocity is directly obtained from (A 1), (A 2), and (38) to be

$$v_s = v_\theta(1,\theta) = \tfrac{1}{2}U\sin\theta - 2\sum_{n=2}^{\infty} B_n^{(2)} \frac{Q_n^{-1/2}(\cos\theta)}{\sin\theta}, \tag{A 3}$$

and $U = -B_2^{(2)}$ to satisfy $D_2^{(2)} = 0$.

The surfactant concentration $\Gamma(\theta)$ is expanded in Legendre polynomials:

$$\Gamma(\theta) = \sum_{m=0}^{\infty} a_m P_m(\cos\theta), \tag{A 4}$$

where $P_m(\cos\theta)$ is the Legendre polynomial of order m.

The solution entails finding the unknown coefficients $B_n^{(2)}$ and a_m. Substituting (A 3) and (A 4) into the surface mass balance (28) and the tangential stress balance (30), two nonlinear equations result:

$$\sum_{m=0}^{\infty} a_m \Bigg[-B_2^{(2)} P_m(\cos\theta)\cos\theta + \tfrac{1}{2}B_2^{(2)} m(m+1)\, Q_{m+1}^{-1/2}(\cos\theta) - 2\sum_{n=2}^{\infty} B_n^{(2)} \left[P_m(\cos\theta)\, P_{n-1}(\cos\theta) - m(m+1)\frac{Q_{m+1}^{-1/2}(\cos\theta)\, Q_n^{-1/2}(\cos\theta)}{\sin^2\theta} \right] + Bik P_m(\cos\theta) + Bi\, P_m(\cos\theta)\exp\left(-\lambda_d y \sum_{m=0}^{\infty} a_m P_m \cos\theta \right) \Bigg] - Bik/y = 0 \tag{A 5}$$

and

$$(1+\tfrac{3}{2}\kappa)(2+\delta)\,E(G\Theta+1)\Bigg[y\Big/\Big(1-y\sum_{m=0}^{\infty}a_m\,P_m(\cos\theta)\Big)$$
$$-\lambda y^2\sum_{m=0}^{\infty}a_m\,P_m(\cos\theta)\Bigg]\sum_{m=0}^{\infty}a_m\,m(m+1)\,Q_{m+1}^{-1/2}(\cos\theta)/\sin\theta$$
$$-3(1+\tfrac{3}{2}\kappa)\sin\theta\Bigg[EG\Bigg(\ln\Big(1-\sum_{m=0}^{\infty}a_m\,P_m(\cos\theta)\,y\Big)+\lambda y^2\Big(\sum_{m=0}^{\infty}a_m\,P_m(\cos\theta)\Big)^2\Big/2\Bigg)-1\Bigg]$$
$$+(1+\kappa)\sum_{n=2}^{\infty}(4n-2)\,B_n^{(2)}\,Q_n^{-1/2}(\cos\theta)/\sin\theta+\tfrac{3}{2}B_2^{(2)}\,\kappa\sin\theta=0. \tag{A 6}$$

Equations (A 5) and (A 6) are solved simultaneously using a multiple collocation technique (Finlayson 1972). The infinite series are truncated to include terms up to a_M and $B_N^{(2)}$. A system of $M+N$ unknowns results, requiring $M+N$ equations for their evaluation, obtained by evaluating (A 5) and (A 6) at $(M+N)/2$ equidistant discrete collocation points along the droplet surface. A set of $M+N$ nonlinear algebraic equations result in terms of the unknown constants:

$$\sum_{m=0}^{M}a_m\Bigg[\Bigg[-B_2^{(2)}\,P_m(\cos\theta_i)\cos\theta_i+\tfrac{1}{2}B_2^{(2)}\,m(m+1)\,Q_{m+1}^{-1/2}(\cos\theta_i)$$
$$-2\sum_{n=2}^{N}B_n^{(2)}\Bigg[P_m(\cos\theta_i)\,P_{n-1}(\cos\theta_i)-m(m+1)\frac{Q_{m+1}^{-1/2}(\cos\theta_i)\,Q_n^{-1/2}(\cos\theta_i)}{\sin^2\theta_i}\Bigg]$$
$$+Bi\,k\,P_m(\cos\theta_i)+Bi\,P_m(\cos\theta_i)\exp\Big(-\lambda_d\,y\sum_{m=0}^{M}a_m\,P_m(\cos\theta_i)\Big)\Bigg]\Bigg]-Bi\,k/y=0 \tag{A 7}$$

and

$$(1+\tfrac{3}{2}\kappa)(2+\delta)\,E(G\Theta+1)\Bigg[y\Big/\Big(1-y\sum_{m=0}^{M}a_m\,P_m(\cos\theta_i)\Big)$$
$$-\lambda y^2\sum_{m=0}^{M}a_m\,P_m(\cos\theta_i)\Bigg]\sum_{m=0}^{M}a_m\,m(m+1)\,Q_{m+1}^{-1/2}(\cos\theta_i)/\sin\theta_i$$
$$-3(1+\tfrac{3}{2}\kappa)\sin\theta_i\Bigg[EG\Bigg(\ln\Big(1-\sum_{m=0}^{M}a_m\,P_m(\cos\theta_i)\,y\Big)+\lambda y^2\Big(\sum_{m=0}^{M}a_m\,P_m(\cos\theta_i)\Big)^2\Big/2\Bigg)-1\Bigg]$$
$$+(1+\kappa)\sum_{n=2}^{N}(4n-2)\,B_n^{(2)}\,Q_n^{-1/2}(\cos\theta_i)/\sin\theta_i+\tfrac{3}{2}B_2^{(2)}\,\kappa\sin\theta_i=0. \tag{A 8}$$

(In these expressions, i denotes the collocation point ($i=1,2,\ldots(N+M)/2$) taken along the droplet surface ($0^\circ<\theta_i<180^\circ$). The equation set is solved by Newton's iteration for the unknown constants a_m and B_n. Initial guesses for the unknowns are obtained by an incremental process. Analytical values for a_0–a_2 and $B_2^{(2)}$–$B_4^{(2)}$ are found from a perturbation study about infinite Bi. At finite large Bi, using small deviations from these values, the remaining coefficients are found to satisfy (A 7) and (A 8). Bi is then reduced incrementally using the converged values of a_m and $B_n^{(2)}$ from the previous Bi as the initial guesses.

The number of collocation points was increased until two convergence criteria were obeyed. The migration velocity (specified by the value of $B_2^{(2)}$) converged to within 10^{-5}:

$$\frac{B_2^{(2)(N,M)} - B_2^{(2)(N-1,M-1)}}{B_2^{(2)(N,M)}} < 10^{-5}, \tag{A 9}$$

and the values of $\Gamma(\theta)$ and $v_s(\theta)$ converged to within 10^{-3} at 37 equally spaced positions (every 5°) on the droplet surface. (In all cases, the collocation points at $\theta_i = 0$ and π are displaced slightly, i.e. $\theta_i = 0$–$0.8°$ and $\pi - 0.8°$).

This procedure works very well for all cases. The required number of collocation points, $(N+M)/2$, increases for small values of E, δ, Bi or $k(< 0.1)$. For example, at $\kappa = 0$, $E = 0.1$, $k = 0.5$, $\lambda = 1$, and $Bi < 0.1$, the maximum number of collocation points required is 84. For the general inviscid bubble case, when Ma, Bi and k are larger than unity, only 16 collocation points are needed. For $\kappa > 0$, fewer points are required for any value of Bi, k and E. Similarly, for large Bi, E, δ or k, fewer points are required. These convergence criteria were further verified by increasing the number of collocation points (sometimes by up to a factor of 4) for several cases. In all cases, the convergence criteria reported here were sufficient to provide converged results to four significant figures for all computed profiles.

In addition to confirming that numerical results fell to expected limits, an additional analytical check was made on the program. Equations (A 7) and (A 8) were integrated numerically at zero E. For this limit, U is unity and an exact analytical solution for $\Gamma(\theta)$ is obtained. Numerical $\Gamma(\theta)$ profiles were confirmed as agreeing with this exact solution.

REFERENCES

Barton, K. D. & Subramanian, R. S. 1990 The migration of liquid drops in a vertical temperature gradient. *J. Colloid Interface Sci.* **133**, 211.

Bratukhin, Y. K. 1976 Thermocapillary drift of a viscous fluid droplet. *NASA Tech. Transl NASA TT* F 17093.

Chen, J. & Stebe, K. 1996 Marangoni retardation of the terminal velocity of a settling droplet: the role of surfactant physico-chemistry. *J. Colloid Interface Sci.* **178**, 144.

Finlayson, B. A. 1972 *The Method of Weighted Residuals and Variational Principles*. Academic.

Happel, H. & Brenner, H. 1973 *Low Reynolds Number Hydrodynamics*. Noordhoof.

Hardy, S. C. 1979 The motion of bubbles in a vertical temperature gradient. *J. Colloid Interface Sci.* **69**, 157.

Hariri, H. H., Nadim, A. & Borhan, A. 1990 Effect of inertia on the thermocapillary velocity of a drop. *J. Colloid Interface Sci.* **140**, 277.

Kim, H. S. & Subramanian, R. S. 1989*a* Thermocapillary migration of a droplet with insoluble surfactant. I. Surfactant cap. *J. Colloid Interface Sci.* **127**, 417.

Kim, H. S. & Subramanian, R. S. 1989*b* Thermocapillary migration of a droplet with insoluble surfactant. II. General case. *J. Colloid Interface Sci.* **130**, 112.

Lacy, L. L., Witherow, W. K., Facemire, B. R. & Nishioka, G. M. 1982 Optical studies of a binary liquid miscibility gap system. *NASA TM*-82494.

Levich, V. G. 1962 *Physicochemical Hydrodynamics*. Prentice Hall.

Lin, S. Y., McKeigue, K. & Maldarelli, C. 1994 Effect of cohesive energies between adsorbed molecules on surfactant exchange processes: Shifting from diffusion control for adsorption to kinetic-diffusive control for re-equilibration. *Langmuir* **10**, 3442.

Nallani, M. & Subramanian, R. S. 1992 Migration of methanol drops in a vertical temperature gradient in a silicone oil. *J. Colloid Interface Sci.* **157**, 24.

Shankar, N. & Subramanian, R. S. 1988 The motion of a gas bubble due to interfacial tension gradients at low to moderate Marangoni numbers. *J. Colloid Interface Sci.* **123**, 512.

STEBE, K. J., LIN, S. Y. & MALDARELLI, C. 1991 Remobilizing surfactant retarded fluid particle interfaces. I. Stress-free conditions at the interfaces of micellar solutions of surfactants with fast sorption kinetics. *Phys. Fluids* A **3**, 3.

STEBE, K. J. & MALDARELLI, C. 1994 Remobilizing surfactant retarded fluid particle interfaces. II. Controlling the surface mobility at interfaces of solutions containing surface active components. *J. Colloid Interface Sci.* **163**, 177.

SUBRAMANIAN, R. S. 1981 Slow migration of a gas bubble in a thermal gradient. *AICHE J.* **27**, 646.

SUBRAMANIAN, R. S. 1983 Thermocapillary migration of bubbles and droplets. *Adv. Space Res.* **3** (5), 145.

SUBRAMANIAN, R. S. 1992 The motion of bubbles and drops in reduced gravity. In *Transport Processes in Bubbles, Drops, and Particles*. Hemisphere.

WOZNIAK, G., SIEKMANN, J. & SRULIJIES, J. 1988 Thermocapillary bubble and drop dynamics under reduced gravity – survey and prospects. *Z. Flugwiss. Weltraumforsch.* **12**, 137.

YOUNG, N. O., GOLDSTEIN, J. S. & BLOCK, M. J. 1959 The motion of bubbles in a vertical temperature gradient. *J. Fluid Mech.* **6**, 350.